Available online at www.sciencedirect.com
SCIENCE DIRECT®
Optics Communications 261 (2006) 322–326
OPTICS COMMUNICATIONS
www.elsevier.com/locate/optcom

# Femtosecond filamentation in air at low pressures. Part II: Laboratory experiments

G. Méchain [a,*], T. Olivier [a], M. Franco [a], A. Couairon [b], B. Prade [a], A. Mysyrowicz [a]

[a] Laboratoire d'Optique Appliquée, ENSTA/École Polytechnique, CNRS UMR 7639, F-91761 Palaiseau Cedex, France
[b] Centre de Physique Théorique, École Polytechnique, CNRS UMR 7644, F-91128 Palaiseau Cedex, France

Received 30 August 2005; received in revised form 15 October 2005; accepted 15 October 2005

**Abstract**

We present experimental studies of filamentation of a femtosecond laser pulse in air at low pressures. The evolution of the filament has been studied by measuring along the propagation axis the conductivity and the sub-THz emission from the plasma channel. We show experimentally that the filamentation process occurs at pressures as low as 0.2 atm in agreement with numerical simulations. Experimental and numerical results [A. Couairon, M. Franco, G. Méchain, T. Olivier, B. Prade, A. Mysyrowicz, Opt. Commun., submitted for publication] are compared and the possible sources of discrepancy are discussed.


*PACS:* 42.25.Bs; 42.65.Jx; 52.38.Hb; 52.70.Ds

*Keywords:* Femtosecond filamentation; Beam-trapping; Laser–plasma interactions; Conductivity measurements

## 1. Introduction

The propagation of femtosecond laser pulses carrying several times the critical power for self-focusing [2] leads to a particular type of propagation called filamentation, which has been studied both theoretically and experimentally during the past decade [3–7]. This filamentation or self-channeling of the beam takes place via a dynamic competition between beam self-focusing due to the optical Kerr effect and beam defocussing due to photo-ionization when the pulse intensity becomes high enough to induce multiphoton absorption. Other effects are involved in this complex dynamics such as diffraction, group velocity dispersion, self-phase modulation and pulse self-steepening, the combination of which leads to a strong pulse restructuring. This is also at the origin of an important spectral broadening (white continuum emission). Filamentation in air allows intense IR femtosecond pulses to propagate over very long distances, reaching hundreds of meters [8–10]. Using appropriate temporal chirps, the onset of the filament as well as its length can be controlled [9,10]. The white light continuum emitted by the filament can be used to probe the atmosphere with LIDAR techniques [11–13]. Moreover, the plasma column created by filamentation has been used to trigger and guide electric discharges and might possibly be used for lighting protection [14–19]. For such applications, vertical propagation should be achieved to high altitudes. Thus, the study of filamentation at low pressures is important.

In this paper, we present laboratory studies of filamentation as a function of pressure, down to 0.2 atm, which corresponds to altitudes higher than 10 km. These filamentation studies have been performed in a single filament configuration. The measurements presented here concern mainly air conductivity measurements [20–22]. However, because we found some disagreements between our results and simulations, we have performed additional measurements using heterodyne radiometric detection in the sub-THz range [23–31]. Both experimental techniques yield similar results.

* Corresponding author. Tel.: +33 1 69 31 97 02; fax: +33 1 69 31 99 96.
*E-mail address:* gregoire.mechain@ensta.fr (G. Méchain).

0030-4018/$ - see front matter © 2005 Elsevier B.V. All rights reserved.
doi:10.1016/j.optcom.2005.11.041

The experimental setup and the methods, procedures and conditions of the measurements are described in Section 2. In Section 3, the data are presented and compared with the numerical studies of Ref. [1]. We focus especially on the behavior of the filament length as a function of pressure.

## 2. Experimental setup and measurement methods

The experimental setup is presented in Fig. 1. The laser system is a Ti:sapphire CPA (Chirp Pulse Amplification) laser system operating at 10 Hz and delivering a maximum output power of 0.2 TW per pulse. The pulse duration has been characterized using an autocorrelation setup and is equal to 130–135 fs (FWHM). The beam at the output of the compressor is roughly Gaussian with a waist equal to 10.4 mm. This beam is truncated by a circular aperture whose radius is equal to 4.5 mm in order to have a more stable beam shape with a perfect circular symmetry. A Galilean telescope further reduces the beam by a factor roughly equal to 2. The final laser beam profile after the telescope has been characterized by a calibrated CCD-camera. Fig. 2 represents this beam profile, fitted by a super-Gaussian profile whose radius at $1/e^2$ is equal to 2.32 mm.

After the telescope, the laser beam is focused inside a tube assembly by using a converging lens having a two meter focal length. The air pressure inside the tube can be controlled from 0.2 to 1 atm. The tube consists in a 1.5 m glass tube followed by metallic tubes of various lengths. A special cell with two electrodes can be inserted to allow conductivity measurements at various distances and pressures. These measurements are performed by recording the electric conduction of the plasma channel using the method described in a previous work [20]. A voltage of 800 V is applied between two copper electrodes drilled in their center and separated by 25 mm (see Fig. 1). The conducting plasma column formed by the self-guided pulse closes the electric circuit. The peak of the induced current between the electrodes is measured through a load resistance $R = 8.2\ \mathrm{k\Omega}$ linked to a fast digital oscilloscope (1-GHz bandwidth). All curves presented here have been obtained using the same procedure. Each point represents the average on three measurements. Each measurement corresponds to the highest value obtained in a consecutive series of 100 laser shots.

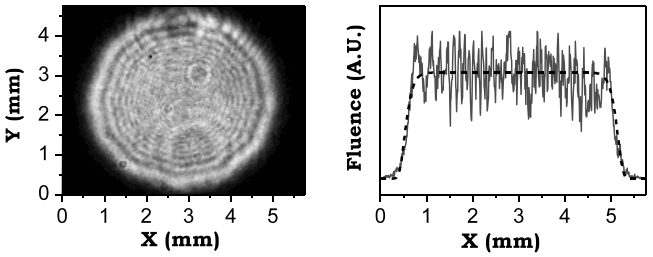


Fig. 2. Left: Beam profile measured with a calibrated CCD camera just before the focusing lens. Right: Fluence profile taken along the horizontal diameter of the beam (solid line) and super-Gaussian fit (dashed line) following the relationship $I(r) \propto \exp[-2(\frac{r}{w_0})^n]$, with $n = 22$ and $w_0 = 2.32$ mm.

The sub-terahertz radiation emitted by the plasma channel has been detected via an heterodyne radiometer. The detailed description of the detector is reported in Ref. [32]. The detection frequency is 91(±3) GHz. The detector is aligned perpendicularly to the plasma channel direction. The emission of the electromagnetic pulse (EMP) is collected inside the corrugated horn of a radiometer with two Teflon lenses, with a focal length equal to 80 mm. The lenses are transparent in the spectral range of interest and have a corrugated structure to avoid reflections. In order to perform the radiometric measurements at different pressures, a cross-shaped tube with two Teflon windows facing one another is used and can be set at different positions along the plasma channel.

In order to correlate the radiometric measurements and the conductivity measurements, we have first compared both signals, pulse after pulse, at a given position (170 cm from the focusing lens) where the conductivity is quite high. The results of these fluctuation and correlation studies is represented in Fig. 3. As can be noticed, the correlation is excellent. Another comparison is performed by measuring the plasma length with both methods (see Fig. 4), showing again good agreement. As a conclusion, the radiometric measurements validate the conductivity measurements. Only the conductivity measurements will be presented in the rest of this paper, since the radiometric measurements have a smaller dynamic range.

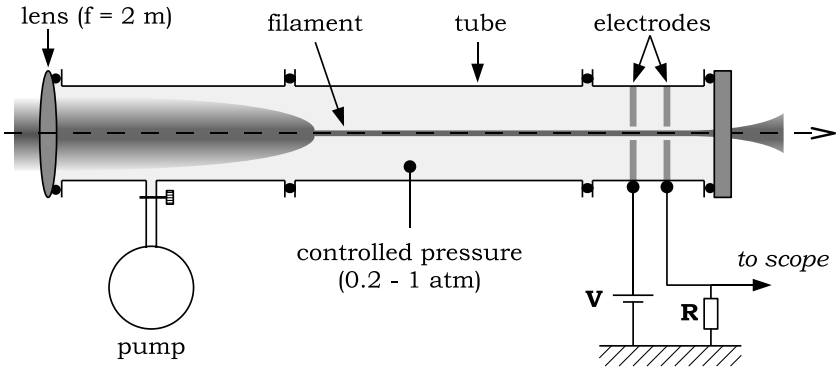


Fig. 1. Experimental setup used for low pressure measurements of the conductivity of the filament.

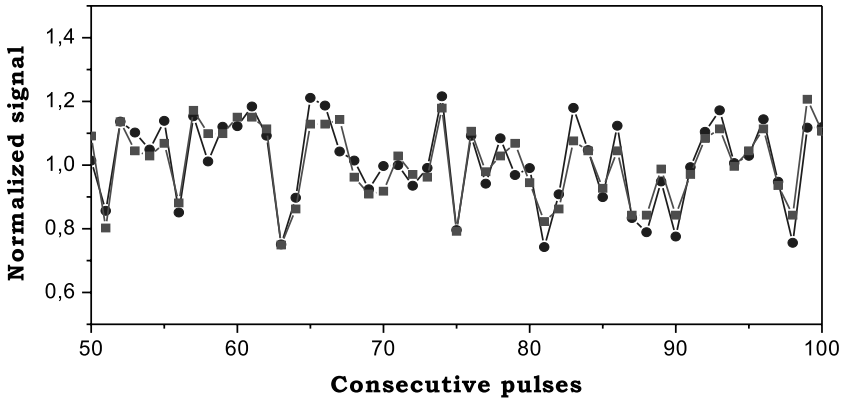


Fig. 3. Measurement of the conductivity (circles) and radiometric heterodyne signal radiated at 91 GHz (squares) recorded simultaneously at the same position.

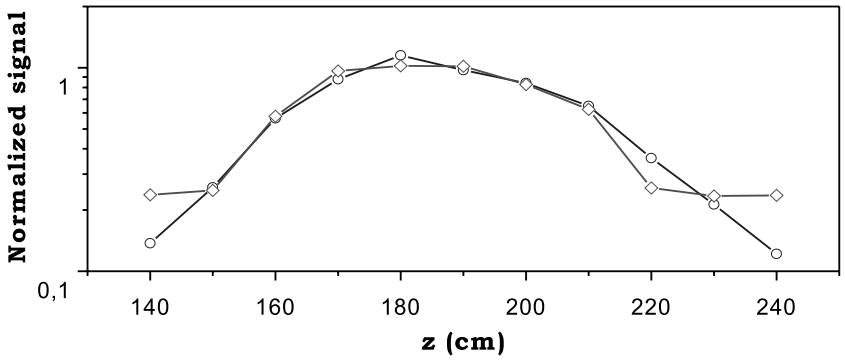


Fig. 4. Filament characterization: Comparison between conductivity measurements and radiometric heterodyne measurements (diamonds = radiometric measurement, circles = conductivity measurement).

## 3. Experimental results and discussion

The measurements, presented in Fig. 5, were performed with an incident energy of 3.7 mJ, which is the maximum energy that produces a single plasma channel. One notices several features. First, the filamentation subsists even at our lowest pressure of 0.2 atm. Second, the maximum signal is clamped to the same value. Finally,

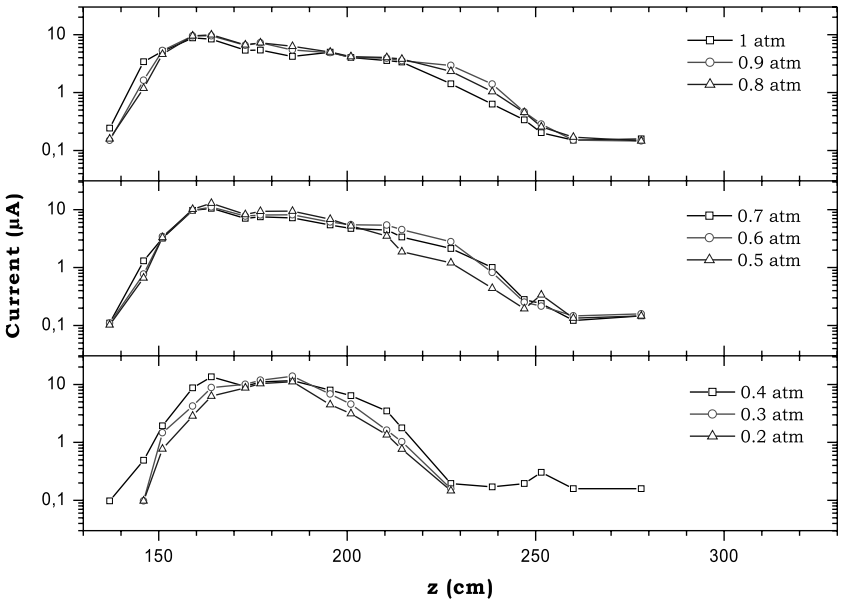


Fig. 5. Evolution of the conductivity of the filament along the optical axis with an energy equal to 3.7 mJ/pulse. $z$ is the distance from the focusing lens. The presented signal corresponds to the current in the load resistance. The measurements have been performed for different pressures inside the tube, varying from 0.2 to 1 atm.

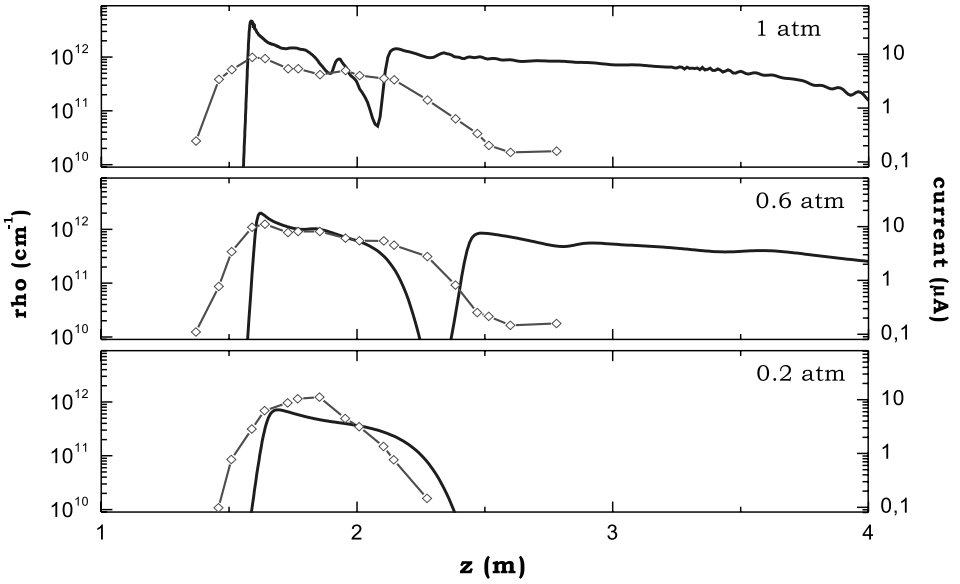


Fig. 6. Comparison between the experimental results at 3.7 mJ (diamonds, scale on the right axis) and numerical simulations (line, scale on the left axis) of the number of electrons per length unit (rho) for 3 pressures (0.2, 0.6 and 1 atm). A super-Gaussian beam profile is used as in Fig. 7.

the total length of the filament diminishes at the lowest pressures.

Using the method and the numerical model described in Ref. [1], we have performed numerical simulations adapted to our experimental setup and conditions. Fig. 6 represents simulations that have been performed for three different representative pressures: 0.2, 0.6 and 1 atm using a super-Gaussian initial beam shape which closely fits the measured beam profile.

We now compare the results of Fig. 5 to the numerical results. In Fig. 6, we plot the experimental results obtained with a pulse energy of 3.7 mJ at three representative pressures together with numerical simulations. As can be seen, the numerical results reproduce well the first portion of the filament including the magnitude of the signal and the location of the start of the filament. The discrepancy concerning the total length of the plasma column for 0.6 and 1 atm appear when we introduce the super-Gaussian input beam in the simulations. A Gaussian input beam, although farther from the experimental input beam leads to a good agreement for the length of the plasma channel. We also note that by reducing the pulse energy by a factor of two with the super-Gaussian beam, the extension of the plasma channel vanishes (see Fig. 7), we retrieve the experimental data. From the observed discrepancy, we conclude first of all that the modulations in the input beam which are produced by the circular aperture have an influence in the dynamics and cannot simply be considered as noise and averaged. Second, the ionization rates in our model are computed from the Keldysh formulation taken in the multiphoton limit. Some authors correct these rates by numerical factors to approach the effective ionization rates [33]. The length of the plasma channel, in particular the presence of a refocusing clearly depend on these rates. A closer inspection of the numerical data explains why the measured air resistivity is approximately constant for all pressures. The diameter of the plasma column increases with decreasing pressure while the on-axis electron density decreases correspondingly, keeping the integrated electron density approximately constant. On the other hand, the experimental signal is proportional to the number of charges integrated over a plasma channel cross-section.

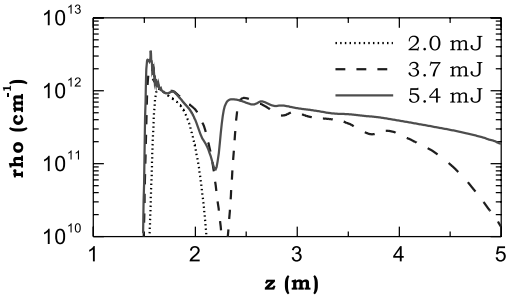


Fig. 7. Numerical simulations of the number of electrons per length unit (rho) for three different incident energies: 2, 3.7 and 5.4 mJ. The pressure is 0.6 atm. A super-Gaussian beam profile, $I(r) \propto \exp[-2(\frac{r}{w_0})^n]$, with $n = 22$ and $w_0 = 2.32$ mm, is used.

## 4. Conclusion

Following the simulations performed in part one, we studied experimentally the behavior of femtosecond light filaments in air at low pressures. The possibility of filamentation in air at pressures as low as 0.2 atm has been demonstrated. This corresponds to a vertical propagation at an altitude greater than 10 km, which is fundamental for LIDAR or lightning triggering applications. Besides, the reduction of the plasma channel length has been observed as the pressure decreases, which validates the simulations performed in Ref. [1]. Experimentally, the effect of the

pressure on the position of the onset of the filament follows that predicted by Marburger's law for the position of the nonlinear focus which is shifted a few cm toward the focus of the lens when pressure decreases to 0.2 atm. In addition, we note both experimentally and theoretically that the maximum conductivity level is clamped to a value that is almost not affected by the pressure variation. The simulations performed with input beams roughly mimicking the experimental intensity profile predict that plasma columns are longer than measured. This discrepancy in the length of the plasma channel indicated that not only the averaged intensity profile could affect the propagation dynamics but also the diffraction rings introduced by the inverse telescope. The ionization rates were also found to play a key role in the formation of an extended plasma channel.

## References

[1] A. Couairon, M. Franco, G. Méchain, T. Olivier, B. Prade, A. Mysyrowicz, Opt. Commun., submitted for publication.
[2] J.H. Marburger, Prog. Quant. Electron. 4 (1975) 35.
[3] A. Braun, G. Korn, X. Liu, D. Du, J. Squier, G. Mourou, Opt. Lett. 20 (1) (1995) 73.
[4] E.T.J. Nibbering, P.F. Curley, G. Grillon, B.S. Prade, M.A. Franco, F. Salin, A. Mysyrowicz, Opt. Lett. 21 (1) (1996) 62.
[5] A. Brodeur, C.Y. Chien, F.A. Ilkov, S.L. Chin, O.G. Kosareva, V.P. Kandidov, Opt. Lett. 22 (5) (1997) 304.
[6] H.R. Lange, G. Grillon, J.-F. Ripoche, M.A. Franco, B. Lamouroux, B.S. Prade, A. Mysyrowicz, E.T.J. Nibbering, A. Chiron, Opt. Lett. 23 (2) (1998) 120.
[7] M. Mlejnek, M. Kolesik, E.M. Wright, J.V. Moloney, Phys. Rev. Lett. 83 (15) (1999) 2938.
[8] B. La Fontaine, F. Vidal, Z. Jiang, C.Y. Chien, D. Comtois, A. Desparois, T.W. Johnston, J.-C. Kieffer, H. Pépin, Phys. Plasmas 6 (1999) 1615.
[9] G. Méchain, A. Couairon, Y.-B. André, C. D'Amico, M. Franco, B. Prade, S. Tzortzakis, A. Mysyrowicz, R. Sauerbrey, Appl. Phys. B 79 (2004) 379.
[10] G. Méchain, C. D'Amico, Y.-B. André, S. Tzortzakis, M. Franco, B. Prade, A. Mysyrowicz, A. Couairon, E. Salmon, R. Sauerbrey, Opt. Commun. 247 (2005) 171.
[11] L. Wöste, C. Wedekind, H. Wille, P. Rairoux, B. Stein, S. Nikolov, C. Werner, S. Niedermeier, F. Ronneberger, H. Schillinger, R. Sauerbrey, Laser Optoelektron. 29 (5) (1997) 51.
[12] P. Rairoux, H. Schillinger, S. Neirdeimer, M. Rodriguez, F. Ronneberger, R. Sauerbrey, B. Stein, D. Waite, C. Wedekind, H. Wille, L. Wöste, C. Ziener, Appl. Phys. B 71 (2000) 573.
[13] M. Rodriguez, R. Bourayou, G. Méjean, J. Kasparian, J. Yu, E. Salmon, A. Scholz, B. Stecklum, J. Eislöffel, U. Laux, A.P. Hatzes, R. Sauerbrey, L. Wöste, J.-P. Wolf, Phys. Rev. E 69 (2004) 036607.
[14] D. Comtois, C.Y. Chien, A. Desparois, F. Génin, G. Jarry, T.W. Johnston, J.-C. Kieffer, B. La Fontaine, F. Martin, R. Mawassi, H. Pépin, F.A.M. Rizk, F. Vidal, P. Couture, H.P. Mercure, C. Potvin, A. Bondiou-Clergerie, I. Gallimberti, J. Appl. Phys. 76 (7) (2000) 819.
[15] B. La Fontaine, D. Comtois, C.Y. Chien, A. Desparois, F. Génin, G. Jarry, T.W. Johnston, J.-C. Kieffer, F. Martin, R. Mawassi, H. Pépin, F.A.M. Risk, F. Vidal, C. Potvin, P. Couture, H.P. Mercure, J. Appl. Phys. 88 (2) (2000) 610.
[16] P. Rambo, J. Schwarz, J.-C. Diels, J. Opt. A 3 (2001) 146.
[17] S. Tzortzakis, B. Prade, M. Franco, A. Mysyrowicz, S. Hüller, P. Mora, Phys. Rev. E 64 (2001) 057401.
[18] M. Rodriguez, R. Sauerbrey, H. Wille, L. Wöste, T. Fujii, Y.-B. André, A. Mysyrowicz, L. Klingbeil, K. Rethmeier, W. Kalkner, J. Kasparian, E. Salmon, J. Yu, J.-P. Wolf, Opt. Lett. 27 (2002) 772.
[19] N. Khan, N. Mariun, I. Aris, J. Yeak, New J. Phys. 4 (61) (2002) 1.
[20] S. Tzortzakis, M.A. Franco, Y.-B. André, A. Chiron, B. Lamouroux, B.S. Prade, A. Mysyrowicz, Phys. Rev. E 60 (1999) R3505.
[21] H. Schillinger, R. Sauerbrey, Appl. Phys. B 68 (1999) 753.
[22] H.D. Ladouceur, A.P. Baronavski, D. Lohrmann, P.W. Grounds, P.G. Girardi, Opt. Commun. 189 (2001) 107.
[23] C.-C. Cheng, E.M. Wright, J.V. Moloney, Phys. Rev. Lett. 97 (2001) 213001 1.
[24] G. Shvets, I. Kaganovich, E. Startsev, Phys. Rev. Lett. 89 (13) (2002) 139301.
[25] C.-C. Cheng, E.M. Wright, J.V. Moloney, Phys. Rev. Lett. 89 (13) (2002) 139302.
[26] V.T. Tikhonchuk, Phys. Rev. Lett. 89 (20) (2002) 209301.
[27] P. Sprangle, J.R. Peñano, B. Hafizi, C.A. Kapetanakos, Phys. Rev. E 69 (6) (2004) 066415.
[28] J.R. Peñano, P. Sprangle, B. Hafizi, A. Ting, D.F. Gordon, C.A. Kapetanakos, Phys. Plasmas 11 (5) (2004) 2865.
[29] W. Hoyer, A. Knorr, J. Moloney, E. Wright, M. Kira, W. Koch, Phys. Rev. Lett. 94 (11) (2005) 115004.
[30] A. Proulx, A. Talebpour, S. Petit, S.L. Chin, Optics Commun. 174 (2000) 305.
[31] G. Méchain, S. Tzortzakis, B. Prade, M. Franco, A. Mysyrowicz, B. Leriche, Appl. Phys. B 77 (2003) 707.
[32] S. Tzortzakis, G. Méchain, G. Palatano, Y.-B. André, M. Franco, B. Prade, A. Mysyrowicz, Opt. Lett. 27 (21) (2002) 1944.
[33] A. Talebpour, J. Yang, S.L. Chin, Opt. Commun. 163 (1–3) (1999) 29.